

# Coded Illumination for Improved Lensless Imaging

Yucheng Zheng and M. Salman Asif

Electrical and Computer Engineering, University of California Riverside

yzhen069@ucr.edu, sasif@ucr.edu

## Abstract

*Mask-based lensless cameras can be flat, thin and light-weight, which makes them suitable for novel designs of computational imaging systems with large surface areas and arbitrary shapes. Despite recent progress in lensless cameras, the quality of images recovered from the lensless cameras is often poor due to the ill-conditioning of the underlying measurement system. In this paper, we propose to use coded illumination to improve the quality of images reconstructed with lensless cameras. In our imaging model, the scene/object is illuminated by multiple coded illumination patterns as the lensless camera records sensor measurements. We designed and tested a number of illumination patterns and observed that shifting dots (and related orthogonal) patterns provide the best overall performance. We propose a fast and low-complexity recovery algorithm that exploits the separability and block-diagonal structure in our system. We present simulation results and hardware experiment results to demonstrate that our proposed method can significantly improve the reconstruction quality.*

## 1. Introduction

Lensless cameras provide novel designs for extreme imaging conditions that require small, thin form factor, large field-of-view, or large-area sensors [2,4,6]. Compared to conventional lens-based cameras, lensless cameras can be flat, thin, light-weight, and potentially flexible because the physical constraints imposed by a lens are relaxed. FlatCam is an example of a lensless camera [4], which belongs to a broader class of coded-aperture cameras that replace the lens with a coded mask [13, 18]. The image formed on the sensor with a coded mask is a linear combination of multiple shifted versions of the scene. To recover the scene image from the sensor measurements, we need to solve a linear inverse problem. The quality of the recovered image depends on the conditioning of the linear system; especially in the absence of any prior knowledge about the scene.

In this paper, we propose a new method that combines coded-illumination with mask-based lensless cameras (such

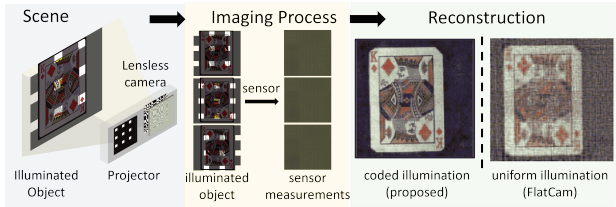


**Figure 1.** An overview of our proposed method. We project a sequence of binary illumination patterns onto the object and capture the measurements for each pattern. The reconstruction result using our method significantly outperforms the conventional method where the scene is illuminated by uniform illumination.

as FlatCam) to improve the quality of recovered images, illustrated by Figure 1. Our main objective is to demonstrate that we can significantly improve the conditioning of lensless imaging systems and the quality of the reconstruction by using coded illumination. The proposed framework can be used to build high-resolution, compact under-the-display fingerprint sensors/cameras that can use display panels for coded illumination [44, 46, 47]. Lensless microscopes [1, 2, 14] can also benefit by combining coded illumination with data capture.

In our proposed method, a 2D scene is illuminated with multiple coded patterns during data acquisition. We capture sensor measurements for each illumination pattern and use a fast recovery algorithm to reconstruct the scene using all the measurements. As we discuss below, a naïve approach would require storing all the images, which increases the storage complexity of the system proportional to the number of illumination patterns. To avoid the increase in the storage cost, we propose a low-complexity algorithm that does not require storing all the images. Instead, we recursively update an estimate of all the matrices and vectors needed for image recovery without any additional storage overhead. Thus, the storage cost of our method remains constant regardless of the number of illumination patterns. Every captured sensor measurement requires some processing, so the computational cost per recovered image increases linearly with the number of illumination patterns. Our experiments show that the image quality improves in almost all cases as we increase the number of illumination patterns. Our method also has an inherent trade-off between

imaging speed and the quality of recovered image.

The main contributions of this paper are as follows

- We propose a framework to combine coded illumination with lensless imaging.
- We propose a fast and low-complexity algorithm that exploits separability of the mask and illumination patterns and avoids storing all the measurements or creating large system matrices during reconstruction.
- We designed shifting dots and orthogonal patterns that provide best overall performance in terms of quality and computational complexity.
- We present simulation results to show that our method can improve the image reconstruction quality under different system conditions.
- We present real experiments using a prototype we built to evaluate the performance of our imaging system and algorithm in the real environments.

## 2. Related Work

Mask-based lensless camera such as FlatCam [4] is an extended version of pinhole cameras. Although a pinhole camera is able to image the scene directly on its sensor, it often suffers from noise [45]. Coded aperture-based cameras alleviate this problem by using multiple pinholes placed in a designed pattern [4, 6, 9, 13, 18]. In contrast to conventional lens-based cameras that capture images of the scene directly, coded mask-based cameras capture linear measurements of the scene and perform reconstruction by solving a linear inverse problem. Coded aperture-based cameras can also recover the depth information of a scene [1–3, 49]. The main advantage of FlatCam is the thin and flat form factor, which also makes the system ill-conditioned and affects the quality of reconstructed images.

Signal recovery from ill-conditioned and under-determined systems is a classical and long-standing problem in signal processing. A number of methods have been proposed to tackle these problems over the decades [11, 21, 38]. An ill-conditioned system is unstable as its solution can change dramatically with tiny perturbations; thus, such a system rarely generates good results in a signal recovery problem. An under-determined system has fewer measurements than the number of unknowns; thus, it admits infinitely many solutions, and one can hardly determine the true solution using only the measurements. A standard approach to deal with ill-conditioned and under-determined systems is to add a signal-dependent regularization term in the recovery problem, which constrains the range of solutions. Popular methods include adding sparse and low-rank priors on the signals [5, 11, 17, 35, 38] and natural-image-like generators prior [7, 24, 28]. Another approach is to capture multiple, diverse measurements of the scene that makes the modified

imaging system well-condition and the reconstruction more accurate [27, 48].

Our proposed approach is an active imaging approach combining coded modulation or structured illumination method with coded aperture imaging [19, 23, 34]. Structured illumination schemes are commonly used for imaging beyond diffraction in microscopy. These schemes use multiple structured illumination patterns to down-modulate high spatial frequencies in a sample into a low-frequency region that can be captured by the microscope [22, 23, 26]. Other active imaging approach includes time-of-flight sensors [25, 39] that estimate the 3D scene by sending out infrared light and measuring its traveling time in reflection. Coded diffraction imaging is used to recover complex-valued wavefront from Fourier measurements [12, 40]. In coded diffraction imaging, the signal of interest gets modulated by a sequence of illumination patterns before the K-space measurements were captured [10, 29, 31]. Ptychography is another related method for capturing high-resolution microscopy images by capturing multiple images of the scene using a sequence of coded illumination patterns [36, 41].

A random illumination patterns-based lensless imaging method with simulations was presented in [50]. In contrast, we designed shifting dots and orthogonal patterns that are significantly superior to random patterns in terms of quality of reconstruction and computational complexity. We provide detailed simulations and experimental results on real data captured with a custom-built prototype.

## 3. Methods

### 3.1. Separable Imaging Model

FlatCam [4] consists of an amplitude mask placed on top of a bare sensor, and every sensor pixel records a linear combination of the entire scene. Suppose the sensor plane is at the origin of the 3D Cartesian coordinates  $(u, v, z)$  and an amplitude mask is placed parallel to the sensor at distance  $d$ . We can model the measurement recorded at sensor pixel  $(u, v)$  as

$$y(u, v) = \int x(u', v', z) \varphi(u', v', u, v, z) du' dv' dz, \quad (1)$$

where  $x(u', v', z)$  represents the intensity and  $\varphi(u', v', u, v, z)$  represents the sensor response of a point source at  $(u', v', z)$ . In this paper, we assume that the scene consists of a single plane at a known depth; therefore, we can ignore the depth parameter and represent the sensor measurements as

$$\begin{aligned} y(u, v) &= \int x(u', v') \varphi(u', v', u, v) du' dv' \\ &\Rightarrow \mathbf{y} = \Phi \mathbf{x}, \end{aligned} \quad (2)$$

where  $\mathbf{x}$  denotes the scene intensity vector,  $\Phi$  denotes the system matrix, and  $\mathbf{y}$  denotes the sensor measurement vector. The computational and memory complexity of the general imaging model in (2) makes it unsuitable for systems with a large number of scene and sensor pixels. We can overcome this challenge in a number of ways; for instance, we can use a separable model as in FlatCam [1, 4] or a convolutional model as in DiffuserCam [2, 32]. We use a separable system in this paper.

A separable mask pattern that is aligned with the sensor grid yields a separable imaging system, which can be represented as

$$y(u, v) = \int \int x(u', v') \varphi_L(u', u) du' \varphi_R(v', v) dv'. \quad (3)$$

The product of  $\varphi_L(u', v)$  and  $\varphi_R(v', v)$  represents the separable system response for point sources along  $u, v$  axes. Let us assume that  $X$  represents an  $n \times n$  image of the scene intensities at a fixed plane and  $Y$  denotes  $m \times m$  sensor measurements, then we can represent the separable system in (3) as

$$Y = \Phi_L X \Phi_R^\top, \quad (4)$$

where  $\Phi_L, \Phi_R$  denote the system matrices for  $u, v$  axes, respectively. We assume square shapes for the scene and sensor to keep our discussion simple, but the ideas can be extended to arbitrary shapes.

### 3.2. Coded Illumination and Reconstruction

The effect of illumination can be modeled as an element-wise product between the scene and the illumination patterns. In our experiments, we use a laser projector placed next to the lensless camera to illuminate the object. In other applications, such as under-the-display camera, an LED screen can be used for illumination. To simplify the recovery process, we further assume that the illumination patterns are separable and drawn from columns of  $n \times k$  matrices  $P_L$  and  $P_R$ . Let us denote a pattern a  $P_{i,j} = p_{Li} p_{Rj}^\top$ , where  $p_{Li}$  and  $p_{Rj}$  are  $i$ th and  $j$ th columns of  $P_L$  and  $P_R$ , respectively. We can describe sensor measurements for any given illumination pattern  $P_{i,j}$  as

$$Y_{i,j} = \Phi_L (P_{i,j} \odot X) \Phi_R^\top, \quad (5)$$

where  $\odot$  represents element-wise multiplication operator.

To recover image  $X$  from the sensor measurements  $Y_{i,j}$ , we can solve the following  $\ell_2$ -regularized problem:

$$\operatorname{argmin}_X \sum_{i,j} \|Y_{i,j} - \Phi_L (P_{i,j} \odot X) \Phi_R^\top\|_2^2 + \lambda \|X\|_2^2, \quad (6)$$

where  $\lambda > 0$  is a regularization parameter. An optimal solution of (6) must satisfy the following conditions

(which can be derived by setting the gradient to zero) with  $\mathbf{Q} = \sum_{i,j} (\Phi_L^\top Y_{i,j} \Phi_R) \odot P_{i,j}$ :

$$\begin{aligned} \mathbf{Q} &= \underbrace{(\Phi_L^\top \Phi_L \odot P_L P_L^\top)}_{\mathbf{A}_L} X \underbrace{(\Phi_R^\top \Phi_R \odot P_R P_R^\top)}_{\mathbf{A}_R} + \lambda X, \\ &\Rightarrow \mathbf{Q} = \mathbf{A}_L X \mathbf{A}_R + \lambda X, \end{aligned} \quad (7)$$

where  $\mathbf{A}_L$ , and  $\mathbf{A}_R$  are  $n \times n$  matrices. The solution of (7) can be written in a closed form using eigen decomposition of  $\mathbf{A}_L, \mathbf{A}_R$  [4, 50] as

$$\hat{X} = \mathbf{V}_L [(\mathbf{V}_L^\top \mathbf{Q} \mathbf{V}_R) ./ (\mathbf{s}_L \mathbf{s}_R^\top + \lambda \mathbf{1} \mathbf{1}^\top)] \mathbf{V}_R^\top, \quad (8)$$

where  $\mathbf{V}_L, \mathbf{V}_R$  denote the eigenvectors and  $\mathbf{s}_L, \mathbf{s}_R$  denote the eigenvalues of  $\mathbf{A}_L, \mathbf{A}_R$ , respectively, and  $./$  denotes elementwise division of entries in two matrices.

The required storage space for all the parameters is  $\mathcal{O}(n^2)$  because  $\mathbf{Q}, \mathbf{A}_L$ , and  $\mathbf{A}_R$  are  $n \times n$  matrices. We only need to compute  $\mathbf{A}_L, \mathbf{A}_R$  once, each of which cost  $\mathcal{O}(mn^2 + kn^2)$ . Eigen decomposition of  $n \times n$  matrices is  $\mathcal{O}(n^3)$ . The most expensive step in our method is computing  $\mathbf{Q}$ , which we can perform by in-place addition of  $(\Phi_L^\top Y_{i,j} \Phi_R) \odot P_{i,j}$  as we acquire measurements for all  $i, j$ . In this manner, we never need to store any of the captured measurement. The complexity of updating  $\mathbf{Q}$  is  $\mathcal{O}(k^2(nm^2 + mn^2))$ .

### 3.3. Choice of Illumination Patterns

One of our goals is to select the  $n \times k$  illumination pattern matrices  $P_L, P_R$  that maximize the quality of reconstruction for fixed  $\Phi_L, \Phi_R$ . The quality of reconstruction in (8) directly depends on the conditioning of the  $\mathbf{A}_L, \mathbf{A}_R$  matrices in (7), which in turn depends on the mask and illumination patterns. One possible approach to improve the conditioning of  $\mathbf{A}_L, \mathbf{A}_R$  is to make them diagonal or diagonally dominant [20], which we can achieve by enforcing same structures in  $P_L P_L^\top, P_R P_R^\top$ .

In principle, we can make  $P_L P_L^\top$  diagonal or even identity by using  $P_L$  as an identity matrix, which requires  $k = n$ . This would be equivalent to scanning the entire scene by illuminating one pixel at a time. We can also make  $P_L P_L^\top$  identity by selecting  $P_L$  as any orthogonal matrix, which also requires  $k = n$ . In a practical scenario, we can only use a small number of illumination patterns; therefore,  $k \ll n$ . Below we discuss how we can get diagonally dominant  $\mathbf{A}_L, \mathbf{A}_R$  using small values of  $k$ .

We propose to use illumination patterns that constitute an orthogonal basis over  $k \times k$  blocks and repeat the same patterns across the entire scene. The simplest example of such patterns is a dot pattern in which two adjacent dots are placed  $k$  scene pixels apart. We can then shift the dot pattern across horizontal and vertical directions, one pixel at a time, to capture  $k^2$  shifting dots patterns. These shifting

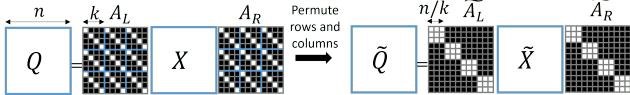


**Figure 2.** Illustration of system in (7) when the illumination patterns form orthogonal basis over  $k \times k$  image patch. (Left)  $A_L$  and  $A_R$  are  $n \times n$  block matrices with diagonal blocks of size  $k \times k$ . (Right) Permuting rows and columns results in block diagonal matrices with block size  $\frac{n}{k} \times \frac{n}{k}$ . The recovery performance of this system depends on the conditioning of each block. We can solve the block diagonal system by recovering  $\frac{n}{k} \times \frac{n}{k}$  patches in  $X$  independently, in parallel.

dots patterns are separable and orthogonal over every  $k \times k$  block. More generally, we can use any sequence of orthogonal separable patterns over  $k \times k$  blocks. Let us assume the separable illumination patterns can be drawn from  $P_L, P_R$  that are defined as

$$P_L = P_R = \begin{bmatrix} \psi_k \\ \vdots \\ \psi_k \end{bmatrix} \Rightarrow P_L P_L^\top = P_R P_R^\top = \begin{bmatrix} I_k & \dots & I_k \\ \vdots & \ddots & \vdots \\ I_k & \dots & I_k \end{bmatrix}, \quad (9)$$

where  $\psi_k$  and  $I_k$  denote  $k \times k$  orthogonal and identity matrices, respectively. The resulting  $P_L P_L^\top, P_R P_R^\top$  matrices (shown above) will be block matrices with  $k \times k$  identity blocks, and the  $\mathbf{A}_L, \mathbf{A}_R$  matrices (shown in Fig. 2) will be block matrices with  $k \times k$  diagonal blocks.

Recall that  $\mathbf{A}_L, \mathbf{A}_R$  are system matrices for the linear system we need to solve in (7). We can permute the rows and columns of  $\mathbf{Q}$ , which is equivalent to permuting rows of  $\mathbf{A}_L$  and columns of  $\mathbf{A}_R$ , without affecting the solution of (7). Let us represent the resulting permuted equations as

$$\tilde{\mathbf{Q}} = \tilde{\mathbf{A}}_L \tilde{\mathbf{X}} \tilde{\mathbf{A}}_R + \lambda \mathbf{X}. \quad (10)$$

We illustrate the permuted system in Fig. 2, where  $\tilde{\mathbf{A}}_L, \tilde{\mathbf{A}}_R$  represent  $n \times n$  block diagonal matrices, with  $k$  blocks along the diagonal each of size  $\frac{n}{k} \times \frac{n}{k}$ .

We can exploit the block diagonal structure of the system matrices to solve the system in (10) in a reliable and computationally efficient manner. Note that the separable, block diagonal system can be divided into  $k^2$  independent systems, each involving an  $\frac{n}{k} \times \frac{n}{k}$  patch in  $\mathbf{X}$ . We can solve all these systems in parallel to speed up recovery. The overall complexity of the inversion also reduces from  $O(n^3)$  to  $O(n^3/k)$ . Furthermore, the conditioning of the overall system now depends on the conditioning of each  $\frac{n}{k} \times nk$  block in  $\tilde{\mathbf{A}}_L, \tilde{\mathbf{A}}_R$ . As long as all the blocks are well-conditioned, we can recover the underlying signal accurately.

## 4. Simulation

### 4.1. Simulation Setup

To validate the performance of the proposed algorithm, we simulate a lensless imaging system where a coded-mask is placed on top of an image sensor. We use a separable

MLS mask pattern. The size of each mask feature is  $60\mu\text{m}$ , and the sensor-mask distance is 2mm. The sensor pitch in the simulation is  $11.72\mu\text{m}$  and the total number of pixels on the sensors is  $512 \times 512$ . We simulate a  $128 \times 128$  planar scene that is 40cm away from the sensor, and the height/width of the scene is 12cm. The simulated sensor noise includes photon noise and read noise, and the noisy sensor measurements can be described as

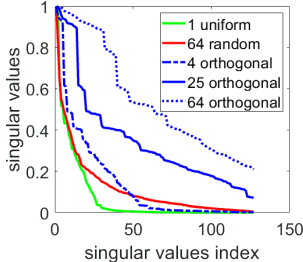
$$\mathbf{Y}_n = \frac{G}{F} (\text{Poisson}(\frac{F}{G} \mathbf{Y}) + N(0, \sigma^2)), \quad (11)$$

where  $\mathbf{Y}$  and  $\mathbf{Y}_n$  refers to original and noisy measurements,  $F$  stands for the full-well capacity, and  $G$  represents the gain value. The variance  $\sigma = F \times 10^{-R/20}$  and  $R$  is the dynamic range. We show the reconstruction results on a few example scenes using different illumination patterns; additional results can be found in the supplementary material.

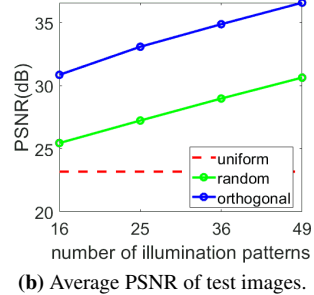
### 4.2. Effect of Illumination on Reconstruction

We first evaluate the conditioning of different illumination patterns by observing the singular values of the system matrices in (7). The matrices that have flat singular value spectrum provide better recovery performance [2, 4, 20]. We tested different types of binary, separable illumination patterns for this experiment. We generate different instances of matrices  $P_L, P_R$  and use outer products of all pairs of columns to generate the illumination patterns. We ensure that the union of all the patterns should illuminate all the pixels (i.e., if we add columns of  $P_L, P_R$ , they should be nonzero everywhere). **Uniform:** One pattern that illuminates all the pixels simultaneously;  $P_L, P_R$  are vectors of all ones. **Random:**  $P_L$  and  $P_R$  are  $k \times n$  binary random matrices that generate  $k^2$  patterns. **Orthogonal:** We tested two types of orthogonal patterns (shifting dots and repeated Hadamard) that yield identical system matrices in (10). **Shifting dots:**  $P_L, P_R$  are  $k \times n$  matrices, each of which consist of  $k \times k$  identity matrices stacked on top of each other (as described in (9)). The base illumination pattern consists of dots separated by  $k$  pixels along the horizontal and vertical directions. We generate a total of  $k^2$  illumination patterns, each of which is a shifted version of the base pattern. The summation of all the patterns will give us a uniform illumination pattern. **Repeated Hadamard:** As an extension to shifting dots,  $P_L, P_R$  are  $k \times n$  matrices, each of which consist of the same  $k \times k$  orthogonal Hadamard matrix stacked on top of each other.

To evaluate the effect of illumination on the lensless imaging system, we observe the decay of singular values of the system matrices in (7) as we increase the number of illumination patterns. Figure 3a plots the singular values for different illumination patterns. The singular values of the original system matrix with one uniform illumination decay sharply. The orthogonal patterns provide significantly better responses compared to random and uniform patterns. As



(a) Singular values of the system.



(b) Average PSNR of test images.

**Figure 3.** Recovery performance of the imaging system. (a) Singular values of the system matrices with 1 uniform, 64 random, and 4, 25, and 64 orthogonal shifting dots patterns. (b) Average PSNR of 8 test images reconstructed with different numbers of illumination patterns. Red dashed line shows results with uniform illumination. Reconstruction quality improves as we increase the number of illumination patterns. The orthogonal patterns outperform random and uniform patterns.

we increase the number of illumination patterns, the singular values spectrum becomes flatter, which corresponds to a system that is nearly orthogonal. In principle, we can use a dot projector to create shifting dots patterns, but we need a programmable projector for Hadamard-like patterns. In our experiments, we use a laser projector for illumination.

We present simulation results for reconstruction of 8 test images using different types and number of illumination patterns in Fig. 3b. We observe that orthogonal patterns outperform other patterns in terms of PSNR. Additional simulation results are available in the supplementary material.

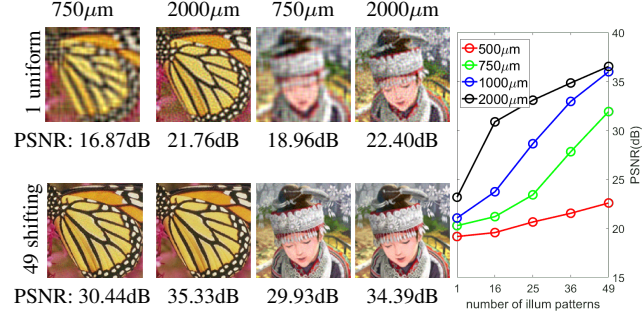
#### 4.3. Effect of Sensor-to-Mask Distance

The sensor-to-mask distance of lensless imaging system greatly influences the conditioning of the system and the quality of reconstruction. We present simulation results to evaluate the performance with different sensor-to-mask distances. We keep the sensor size fixed with  $512 \times 512$  pixels, and test the sensor-to-mask distance at  $500\mu\text{m}$ ,  $750\mu\text{m}$ ,  $1000\mu\text{m}$ , and  $2000\mu\text{m}$ . The reconstruction results for two test images are presented in Fig. 4, along with the PSNR plot for different numbers of shifting dots patterns. We observe that multiple coded illumination patterns outperform the results with a single uniform pattern at all the sensor-to-mask distances. Even if the sensor-to-mask distance is  $750\mu\text{m}$ , the results with 25 coded illumination patterns are comparable to the uniform illumination results at  $2000\mu\text{m}$ . Additional simulation results are available in the supplementary material.

### 5. Experiments

#### 5.1. Experiment Setup

We build a prototype with a lensless camera and a Sony MP-CL1 laser projector, shown in Fig. 5. The lensless camera prototype consists of an image sensor with a coded mask on top of it. The mask has a separable MLS pattern de-



(a) Examples of reconstructed images with sensor-to-mask distance at  $750\mu\text{m}$  and  $2000\mu\text{m}$ .

(b) Average PSNR of 8 test images.

**Figure 4.** Simulation results for reconstruction with different sensor-to-mask distances. The reconstruction quality improves as the sensor-to-mask distance increases.

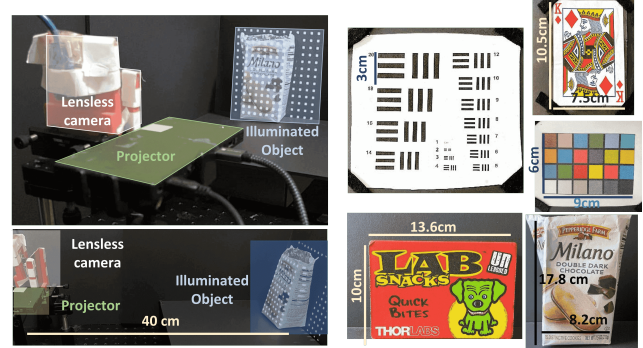


**Figure 5.** The experiment setup and five test scenes (annotated and scaled to proportional size). The projector is placed right next to the lensless camera. The target scenes/objects are 40cm away from the camera.

scribed in [4]. The mask has  $511 \times 511$  square features, each of length/width  $60\mu\text{m}$ . The sensor-mask distance is 2mm. We use a Sony IMX249 sensor that has  $1920 \times 1200$  pixels with  $5.86\mu\text{m}$  pixel pitch. We bin  $2 \times 2$  sensor pixels and record  $512 \times 512$  measurements from the center of the sensor. The effective sensor pitch is  $11.72\mu\text{m}$  and the effective sensor area is nearly  $6 \times 6\text{mm}$ . The target objects are 40cm away from the camera and projector illuminates  $12 \times 12\text{cm}$  area on the scene plane. To reduce the noise and the artifacts caused by the projector refresh cycles, we average 40 instances for each measurement. Finally, we reconstruct  $128 \times 128$  pixels in the illuminated area, which results in the effective resolution of the reconstructed images at  $120\text{mm}/128=0.93\text{mm}$  per pixel.

In our experiment, the pixel grid of the scene, illumination patterns  $P_L$ ,  $P_R$ , the system matrices  $\Phi_L$ ,  $\Phi_R$  must be correctly aligned; otherwise, we will get artifacts in the reconstruction. To avoid any grid mismatch, we use the same projector to calibrate the system matrices and generate the illumination patterns in our experiments. We first calibrate the system matrices by projecting Hadamard patterns on a plane with a dark background and recording the measurements of the projected patterns, then compute  $\Phi_L$ ,  $\Phi_R$  from

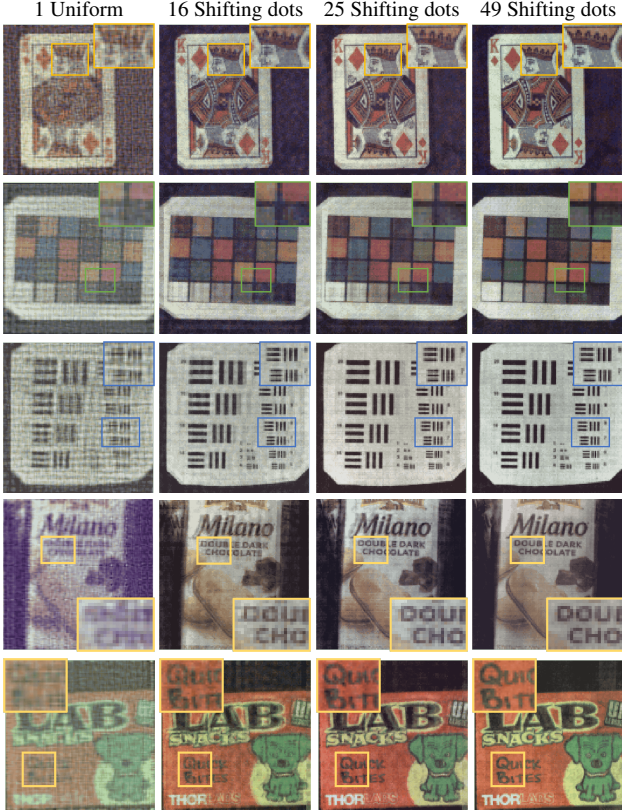


**Figure 6.** Experimental results on five test scenes with different numbers of shifting dots patterns. The reconstruction results using multiple coded illumination patterns outperform the standard lensless camera with uniform illumination. The quality of reconstruction gradually increases as the number of illumination patterns increases.

these measurements using the method described in [4]. Finally, we conduct the experiments with coded illumination while the position and angle of the projector are fixed. This ensures that the pixel grids of the projector and the transfer matrices are identical.

## 5.2. Effect of Illumination Patterns

We present experimental results of our method on five different scenes in Fig. 6 and Fig. 7. The first three rows are printed card, color board, and a resolution target on sheets of paper. Since these scenes are planar, they fit the 2D scene assumption of our model perfectly. The last two rows are real objects with depth variations and may cause depth mismatch in reconstruction.

From the results in Fig. 6, we observe that a single uniform illumination provides poor reconstruction. As we increase the number of illumination patterns, the resolution of the reconstruction images improves significantly. For example, in the third row, the horizontal and vertical features that cannot be resolved with the uniform illumination are easily resolved with the 49 patterns. Also, we observe in the fourth row that, the letters on the cookie bag that are com-

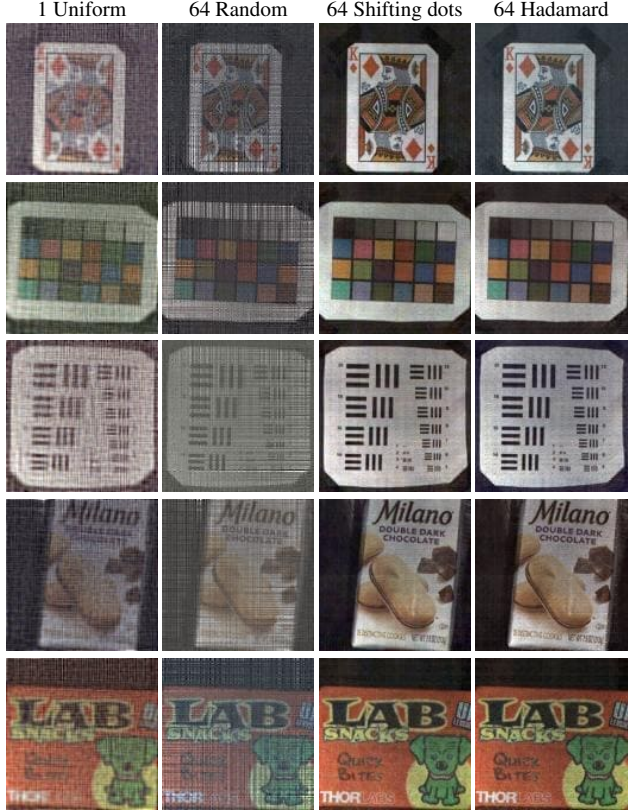


**Figure 7.** Experimental results on five test scenes with different types of illumination patterns. The orthogonal patterns (shifting dots, hadamard) outperform random patterns.

pletely unrecognizable with uniform illumination become very clear with 49 illumination patterns. The last two rows also suggest that our method is robust to small variations in depth. From the results in Fig. 7, the repeated orthogonal patterns(shifting dots and Hadamard) outperform other patterns, as expected from the singular values in Fig. 3a.

Note that neighbouring pixels have a similar response on the sensor in the lensless imaging system; therefore, neighbouring pixels are harder to resolve compared to two pixels that are far from each other. The shifting dots pattern is a dot array where the illuminated pixels are maximally separated; therefore, two neighbouring pixels in the scene are not illuminated at the same time. As we increase the number of shifting dots patterns, the distance between adjacent illuminated pixels also increases, and that provides better reconstruction. Hadamard patterns provide similar separation because of their orthogonal structure.

In summary, the ill-conditioned system matrices with uniform illumination pattern cause various artifacts. Capturing measurements from coded illumination improves the conditioning of the overall system and the resulting reconstructed images contain much lesser artifacts and noise. More illumination patterns demand more acquisition time, which enforces a trade off between the quality of recon-

struction and data acquisition time.

### 5.3. Effective Resolution of Reconstruction

The third row in Fig. 6 has a printed resolution target image with horizontal and vertical features of different widths. We use this image to analyze the resolution of our method empirically. The resolution of our imaging system is determined by the resolution of the projector. We place the target scene 40cm away from the camera and projector. The resolution of MP-CL1 projector is  $1280 \times 720$  and the maximum illuminating area at 40cm throw distance is  $22 \times 13\text{cm}$ . The pixel pitch of projector is 0.17mm, which determines the achievable resolution of our method with the MP-CL1 projector. In our experiment, the width of every reconstructed pixel is 0.93mm, and the angular resolution of our system is  $0.27^\circ$ . We can select smaller pixel pitch by dividing the illuminating area into more pixels, but the pixel pitch cannot be smaller than the lower-bound determined by the projector.

We validate the resolution of our system with the target scene in Fig. 6. We invert the black and white color for better illustration by subtracting the image from 1. The distance between two printed white stripes in group 20 (upper-left) is 7.5mm (0.13 lp/mm) and the distance between two white stripes in group 5 is 1.9mm (0.52 lp/mm). We plot the intensity values of the horizontal line stripes from multiple groups in Fig. 8, where the peaks and valleys correspond to the white and black stripes of the horizontal line pairs. We observe that the line pairs of group 12 can be distinguished clearly while the line pairs of group 3 cannot be distinguished. We also calculate the modulation transfer function (MTF) of the reconstruction from different numbers of illumination patterns in Fig. 8. MTF measures how well we can discern the intensity of bright and dark pixels in line pairs under different conditions [43]. To plot the MTF, we manually select each groups of horizontal line pairs after subtracting a fixed DC background, then average every group along the columns and finally compute the contrast percentage as  $\frac{I_{\max} - I_{\min}}{I_{\max} + I_{\min}} \times 100$ . We observe from the MTF plots that the contrast ratio for all the resolution groups improves as we increase the number of illumination patterns.

### 5.4. Compressive Sensor Measurements

One potential application of coded illumination with lensless imaging is to expand the space of sensor measurements without increasing the number of sensor pixels. This can be especially useful when sensors capture fewer measurements than the number of pixels we seek to recover. Compressive sensing often deals with such scenarios where the number of sensor pixels is smaller than the number of unknown scene pixels [11, 17]. The system becomes under-determined and the reconstruction quality becomes worse. In lensless imaging systems, the number of sensor measurements are often larger than the number of reconstruction

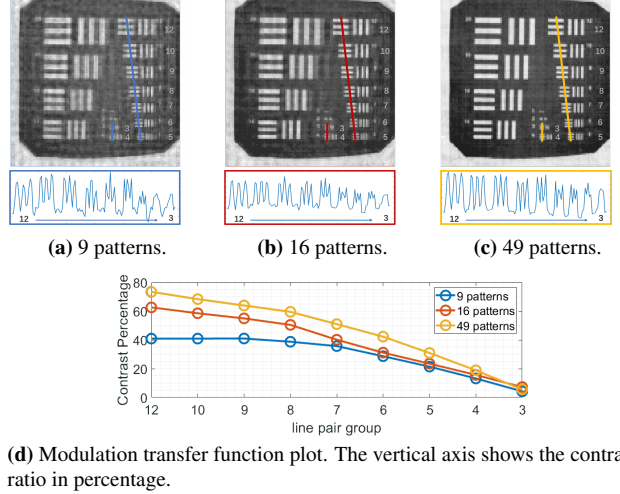


**Figure 8.** Resolution analysis of coded illumination. Top images in (a,b,c) show resolution target reconstructed using 9, 16, and 49 shifting dots patterns. Bottom plots in (a,b,c) show the intensity of a line from group 12 to group 3. The MTF (modulation transfer function) plot for different numbers of shifting dots illumination patterns is shown in (d).

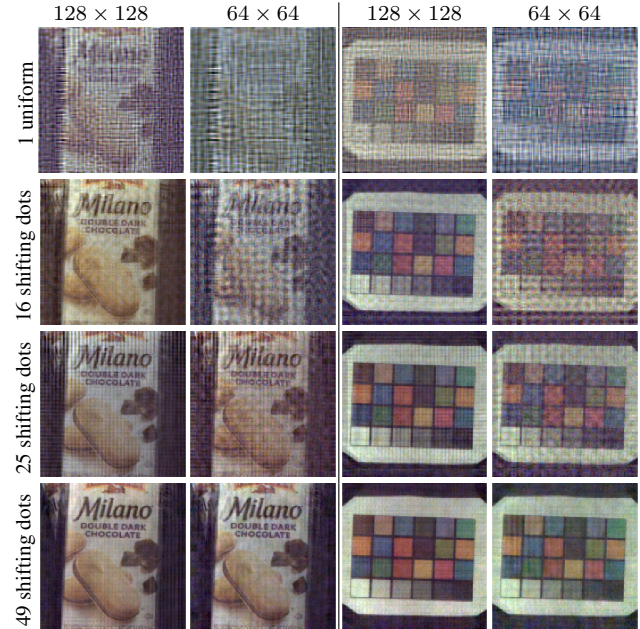


**Figure 9.** Experimental results for reconstructing the  $128 \times 128$  images from  $64 \times 64$  and  $128 \times 128$  measurements. Single (uniform) illumination-based method fails to recover images as the number of measured pixels reduce. Our method with 49 shifting dots patterns recovers near-perfect reconstruction at different levels of binning (compression) factors.

pixels, but that comes at the expense of low resolution of reconstructed images or larger and more costly sensors.

To validate the robustness of our method in under-determined system, we performed an experiment by binning the sensor measurements at increasing factors. The results are presented in Fig. 9. In our experiments, we capture  $512 \times 512$  measurements and bin them to  $256 \times 256$ ,

$128 \times 128$ , or  $64 \times 64$  pixels by averaging the neighbouring pixels in post-processing. The reconstruction image has  $128 \times 128$  pixels, which implies the  $64 \times 64$  sensor measurements yield an under-determined system with one illumination. We present the result of two scenes with different binning factors. We observe that as we bin larger number of pixels, the system with a single uniform illumination becomes ill-conditioned and the quality of reconstruction degrades. On the other hand, the system with 49 shifting dots patterns provides stable reconstruction even when the measurements are binned to  $64 \times 64$  pixels.

### 5.5. Effect of Deep Network Denoising

Deep learning-based methods have been widely used for image recovery and enhancement tasks [16, 30, 33]. For instance, UNet [37] is used for image denoising and removing artifacts from reconstructed images. UNet-based networks have been used to recover photorealistic images from lensless measurements in [30]. Deep learning is also used as the priors to improve the reconstruction results [8], especially when the number of measurements is small.

To test the performance of UNet-based enhancement networks on our lensless imaging setup, we trained a UNet that accepts the reconstruction from a lensless camera as an input and produces a potentially refined image. We created the dataset by simulating the noisy lensless measurements using 500 natural RGB images from [15] with the calibrated transfer matrices  $\Phi_L, \Phi_R$  described in Sec.5.1. Then we reconstruct these measurements using least-squares method in (7). We used the reconstructed images as the input and the original (ground truth) images as the output to the UNet; then we trained the UNet in an end-to-end manner. We used RMSprop optimizer [42] with learning rate of 0.0001 and momentum of 0.9, and trained the UNet for 200 epochs.

We present the results of UNet enhancement in Fig. 10, which suggest that UNet can produce cleaner images but cannot improve the resolution. The images reconstructed from the least-squares method in (7) are presented in “before UNet” column. The images refined by passing through UNet are shown in “after UNet” column. We observe that UNet can successfully reduce the artifacts and noise in the reconstructed images, but fails to improve the spatial resolution. For example, the text in zoomed-in regions is not resolvable in the images before and after UNet for Uniform illumination. In contrast, our proposed method with multiple coded illumination significantly improved the resolution and reduced the noise in the reconstructed image.

## 6. Conclusion and Discussion

We propose a framework for combining coded illumination with lensless imaging. We present extensive simulation and real experiment results to demonstrate that we can get

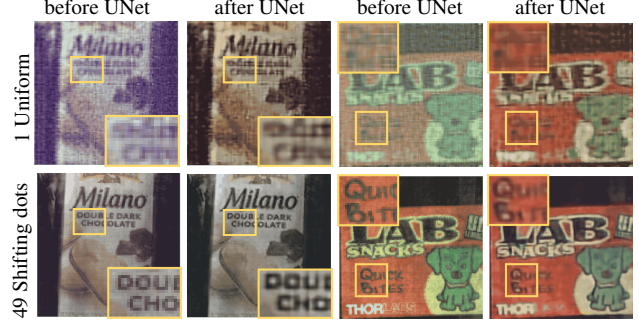


**Figure 10.** Reconstruction of our proposed method with and without a deep denoising network. UNet can produce cleaner images but fails to improve the resolution. Our proposed method with multiple coded illumination patterns significantly improves the resolution of reconstruction.

significantly improved reconstruction with multiple coded illumination compared to original uniform illumination.

### Advantages.

- Qualitative experiment results show that our method has robust performance even if the original system is severely ill-conditioned (small sensor-mask distance and small number of measurements).
- In space-limited applications such as under-the-display sensing, where the sensor-to-mask distance has to be small, our proposed method can offer significantly better reconstruction compared to uniform illumination.
- Our proposed reconstruction algorithm is efficient in both space and time. For shifting dots (and any other orthogonal) pattern over  $k \times k$  blocks, the system can be transformed into  $k^2$  independent small problems that can be solved in parallel for faster and better reconstruction.
- Shifting dots patterns have a simple structure but provide the best results in our experiments. Shifting dots patterns can be easier to implement because all the patterns are simply the shifted copies of the same base pattern.
- Orthogonal patterns would provide similar gains as shifting dots with potentially better light throughput (at the expense of complex hardware).

### Limitations.

- The field-of-view and resolution of reconstructed images are limited by the resolution of illumination patterns.
- Coded illumination hardware can bring additional cost and complexity to the system design.
- Our current system cannot capture dynamic scenes because our model requires multiple measurements of every scene under different illumination patterns.
- The shifting dots patterns are simple and easy to implement, but they reduce the light throughput.
- The camera and projector are co-located in our setup; therefore coded illumination does not provide a direct advantage toward depth estimation. Reconstruction of 3D and dynamic scenes are worthy future directions.

**Negative societal impact.** None expected, apart from a

caution that we have to be careful in reporting and evaluating the performance of computational imaging systems because most of the results are qualitative and come from custom prototypes. Reproducible computational imaging designs can mitigate this concern.

**Acknowledgments.** The authors acknowledge Rongjia Zhang’s help with initial simulations. This work is supported by National Science Foundation (NSF) (CCF-2046293) and Air Force Office of Scientific Research (AFOSR) (FA9550-21-1-0330).

**Supplementary material.** Additional simulation and experimental results are available at <https://github.com/CSIPlab/codedcam>.

## References

[1] Jesse K. Adams, Vivek Boominathan, Benjamin W. Avants, Daniel G. Vercosa, Fan Ye, Richard G. Baraniuk, Jacob T. Robinson, and Ashok Veeraraghavan. Single-frame 3d fluorescence microscopy with ultraminiature lensless flatscope. *Science Advances*, 3(12), 2017. [1](#), [2](#), [3](#)

[2] Nick Antipa, Grace Kuo, Reinhard Heckel, Ben Mildenhall, Emrah Bostan, Ren Ng, and Laura Waller. Diffusercam: lensless single-exposure 3d imaging. *Optica*, 5(1):1–9, Jan 2018. [1](#), [2](#), [3](#), [4](#)

[3] M. Salman Asif. Lensless 3d imaging using mask-based cameras. In *2018 IEEE International Conference on Acoustics, Speech and Signal Processing (ICASSP)*, pages 6498–6502, 2018. [2](#)

[4] M. Salman Asif, Ali Ayremlou, Aswin Sankaranarayanan, Ashok Veeraraghavan, and Richard G. Baraniuk. Flatcam: Thin, lensless cameras using coded aperture and computation. *IEEE Transactions on Computational Imaging*, 3(3):384–397, 2017. [1](#), [2](#), [3](#), [4](#), [5](#), [6](#)

[5] Richard G. Baraniuk. Compressive sensing [lecture notes]. *IEEE Signal Processing Magazine*, 24(4):118–121, 2007. [2](#)

[6] Vivek Boominathan, Jesse K Adams, M Salman Asif, Benjamin W Avants, Jacob T Robinson, Richard G Baraniuk, Aswin C Sankaranarayanan, and Ashok Veeraraghavan. Lensless imaging: A computational renaissance. *IEEE Signal Processing Magazine*, 33(5):23–35, 2016. [1](#), [2](#)

[7] Ashish Bora, Ajil Jalal, Eric Price, and Alexandros G. Dimakis. Compressed sensing using generative models. In *Proceedings of the 34th International Conference on Machine Learning - Volume 70*, ICML’17, pages 537–546. JMLR.org, 2017. [2](#)

[8] Ashish Bora, Ajil Jalal, Eric Price, and Alexandros G. Dimakis. Compressed sensing using generative models. In Doina Precup and Yee Whye Teh, editors, *Proceedings of the 34th International Conference on Machine Learning*, volume 70 of *Proceedings of Machine Learning Research*, pages 537–546. PMLR, 06–11 Aug 2017. [8](#)

[9] Axel Busboom, Harald Elders-Boll, and Hans D. Schotten. Uniformly redundant arrays. *Experimental Astronomy*, 8(2):97–123, Jun 1998. [2](#)

[10] Emmanuel J. Candès, Xiaodong Li, and Mahdi Soltanolkotabi. Phase retrieval from coded diffraction patterns. *Applied and Computational Harmonic Analysis*, 39(2):277–299, 2015. [2](#)

[11] Emmanuel J. Candès, Justin K. Romberg, and Terence Tao. Stable signal recovery from incomplete and inaccurate measurements. *Communications on Pure and Applied Mathematics*, 59(8):1207–1223, 2006. [2](#), [7](#)

[12] Emmanuel J. Candès, Thomas Strohmer, and Vladislav Voroninski. Phaselift: Exact and stable signal recovery from magnitude measurements via convex programming. *Communications on Pure and Applied Mathematics*, 66(8):1241–1274, 2013. [2](#)

[13] Thomas M. Cannon and Edward E. Fenimore. Coded Aperture Imaging: Many Holes Make Light Work. *Optical Engineering*, 19:283, June 1980. [1](#), [2](#)

[14] Nadya Chakrova, Rainer Heintzmann, Bernd Rieger, and Sjoerd Stallinga. Studying different illumination patterns for resolution improvement in fluorescence microscopy. *Opt. Express*, 23(24):31367–31383, Nov 2015. [1](#)

[15] Giorgi Chaladze and Levan kalatozishvili. Linnaeus 5 dataset, Nov 2017. [8](#)

[16] Julie Chang and Gordon Wetzstein. Deep optics for monocular depth estimation and 3d object detection. In *Proc. IEEE ICCV*, 2019. [8](#)

[17] David L. Donoho. Compressed sensing. *IEEE Transactions on Information Theory*, 52(4):1289–1306, April 2006. [2](#), [7](#)

[18] Edward E. Fenimore and Thomas M. Cannon. Coded aperture imaging with uniformly redundant arrays. *Appl. Opt.*, 17(3):337–347, Feb 1978. [1](#), [2](#)

[19] David Fofi, Tadeusz Sliwa, and Yvon Voisin. A comparative survey on invisible structured light. In *IST/SPIE Electronic Imaging*, 2004. [2](#)

[20] Gene H. Golub and Charles F. Van Loan. *Matrix Computations*. The Johns Hopkins University Press, third edition, 1996. [3](#), [4](#)

[21] Gene H. Golub and Charles F. Van Loan. *Matrix Computations (3rd Ed.)*. Johns Hopkins University Press, Baltimore, MD, USA, 1996. [2](#)

[22] Mats G L Gustafsson. Surpassing the lateral resolution limit by a factor of two using structured illumination microscopy. *Journal of microscopy*, 198 Pt 2:82–7, 2000. [2](#)

[23] Mats G L Gustafsson, Lin Shao, Peter M Carlton, C J Rachel Wang, Inna N Golubovskaya, W Zacheus Cande, David A Agard, and John W Sedat. Three-Dimensional Resolution Doubling in Wide-Field Fluorescence Microscopy by Structured Illumination. *Biophysical Journal*, 94:4957–4970, June 2008. [2](#)

[24] Paul Hand, Oscar Leong, and Vlad Voroninski. Phase retrieval under a generative prior. In S. Bengio, H. Wallach, H. Larochelle, K. Grauman, N. Cesa-Bianchi, and R. Garnett, editors, *Advances in Neural Information Processing Systems 31*, pages 9136–9146. Curran Associates, Inc., 2018. [2](#)

[25] Felix Heide, Matthias B Hullin, James Gregson, and Wolfgang Heidrich. Low-budget transient imaging using photonic mixer devices. *ACM Transactions on Graphics (ToG)*, 32(4):45, 2013. [2](#)

[26] Rainer Heintzmann and Christoph G. Cremer. Laterally modulated excitation microscopy: improvement of resolution by using a diffraction grating. In Irving J. Bigio, Herbert

Schneckenburger, Jan Slavik, Katarina Svanberg M.D., and Pierre M. Viallet, editors, *Optical Biopsies and Microscopic Techniques III*, volume 3568, pages 185 – 196. International Society for Optics and Photonics, SPIE, 1999. 2

[27] Yi Hua, Shigeki Nakamura, M. Salman Asif, and Aswin C. Sankaranarayanan. Sweepcam — depth-aware lensless imaging using programmable masks. *IEEE Transactions on Pattern Analysis and Machine Intelligence*, 42(7):1606–1617, 2020. 2

[28] Rakib Hyder, Viraj Shah, Chinmay Hegde, and M. Salman Asif. Alternating phase projected gradient descent with generative priors for solving compressive phase retrieval. In *IEEE International Conference on Acoustics, Speech and Signal Processing (ICASSP)*, pages 7705–7709, 2019. 2

[29] Gauri Jagatap, Zhengyu Chen, Seyedehsara Nayer, Chinmay Hegde, and Namrata Vaswani. Sample efficient fourier ptychography for structured data. *IEEE Transactions on Computational Imaging*, 6:344–357, 2020. 2

[30] Salman Khan, Adarsh R, Vivek Boominathan, Jasper Tan, Ashok Veeraraghavan, and Kaushik Mitra. Towards photorealistic reconstruction of highly multiplexed lensless images. In *IEEE/CVF International Conference on Computer Vision (ICCV)*, pages 7859–7868, 2019. 8

[31] Jianwei Miao, Tetsuya Ishikawa, Qun Shen, and Thomas Earnest. Extending x-ray crystallography to allow the imaging of noncrystalline materials, cells, and single protein complexes. *Annual Review of Physical Chemistry*, 59(1):387–410, 2008. PMID: 18031219. 2

[32] Kristina Monakhova, Kyrollos Yanny, Neerja Aggarwal, and Laura Waller. Spectral diffusercam: lensless snapshot hyperspectral imaging with a spectral filter array. *Optica*, 7(10):1298–1307, Oct 2020. 3

[33] Kristina Monakhova, Joshua Yurtsever, Grace Kuo, Nick Antipa, Kyrollos Yanny, and Laura Waller. Learned reconstructions for practical mask-based lensless imaging. *Opt. Express*, 27(20):28075–28090, Sep 2019.

[34] Shree K. Nayar and Mohit Gupta. Diffuse structured light. In *2012 IEEE International Conference on Computational Photography (ICCP)*, pages 1–11, April 2012. 2

[35] Benjamin. Recht, Maryam. Fazel, and Pablo A. Parrilo. Guaranteed minimum-rank solutions of linear matrix equations via nuclear norm minimization. *SIAM Review*, 52(3):471–501, 2010. 2

[36] John M. Rodenburg. Ptychography and related diffractive imaging methods. volume 150 of *Advances in Imaging and Electron Physics*, pages 87–184. Elsevier, 2008. 2

[37] Olaf Ronneberger, Philipp Fischer, and Thomas Brox. U-net: Convolutional networks for biomedical image segmentation. In *MICCAI*, pages 234–241, 2015. 8

[38] Leonid I. Rudin, Stanley Osher, and Emad Fatemi. Nonlinear total variation based noise removal algorithms. *Phys. D*, 60(1-4):259–268, Nov. 1992. 2

[39] Cyrus Bamji S. Burak Gokturk, Hakan Yalcin. A time-of-flight depth sensor - system description, issues and solutions. In *Conference on Computer Vision and Pattern Recognition Workshop*, pages 35–35, June 2004. 2

[40] Yoav Shechtman, Yonina C. Eldar, Oren Cohen, Henry Nicholas Chapman, Jianwei Miao, and Mordechai Segev. Phase retrieval with application to optical imaging: A contemporary overview. *IEEE Signal Processing Magazine*, 32(3):87–109, 2015. 2

[41] Lei Tian, Xiao Li, Kannan Ramchandran, and Laura Waller. Multiplexed coded illumination for fourier ptychography with an led array microscope. *Biomed. Opt. Express*, 5(7):2376–2389, Jul 2014. 2

[42] T. Tieleman and G. Hinton. Lecture 6.5—RmsProp: Divide the gradient by a running average of its recent magnitude. COURSERA: Neural Networks for Machine Learning, 2012. 8

[43] Charles S. Williams and Orville A. Becklund. *Introduction to the Optical Transfer Function*. 1989. 7

[44] Anqi Yang and Aswin C. Sankaranarayanan. Designing display pixel layouts for under-panel cameras. *IEEE Trans. Pattern Analysis and Machine Intelligence (TPAMI) / Special Issue of ICCP*, 43(7):2245–2256, July 2021. 1

[45] Adam Yedidia, Christos Thrampoulidis, and Gregory Wornell. Analysis and optimization of aperture design in computational imaging. *IEEE International Conference on Acoustics, Speech, and Signal Processing*, pages 4029–4033, April 2018. 2

[46] Ping-Hung Yin, Chih-Wen Lu, Jia-Shyang Wang, Keng-Li Chang, Fu-Kuo Lin, Chia-Jung Chang, and Gen-Chiuan Bai. A  $368 \times 184$  optical under-display fingerprint sensor with global shutter and high-dynamic-range operation. In *2020 IEEE Custom Integrated Circuits Conference (CICC)*, pages 1–4, 2020. 1

[47] Tomoyuki Yokota, Kenjiro Fukuda, and Takao Someya. Recent progress of flexible image sensors for biomedical applications. *Advanced Materials*, 33(19):2004416, 2021. 1

[48] Yucheng Zheng, Yi Hua, Aswin C Sankaranarayanan, and M Salman Asif. A simple framework for 3d lensless imaging with programmable masks. In *Proceedings of the IEEE/CVF International Conference on Computer Vision*, pages 2603–2612, 2021. 2

[49] Yucheng Zheng and M. Salman Asif. Joint image and depth estimation with mask-based lensless cameras. *IEEE Transactions on Computational Imaging*, 6:1167–1178, 2020. 2

[50] Yucheng Zheng, Rongjia Zhang, and M. Salman Asif. Coded illumination and multiplexing for lensless imaging. In *IEEE International Conference on Acoustics, Speech and Signal Processing (ICASSP)*, pages 9250–9253, 2020. 2, 3